Measurement of the Neutrino Mass Splitting and Flavor Mixing by MINOS

P. Adamson,[7] C. Andreopoulos,[20] R. Armstrong,[12] D. J. Auty,[24] D. S. Ayres,[1] C. Backhouse,[18] G. Barr,[18] M. Bishai,[3] A. Blake,[5] G. J. Bock,[7] D. J. Boehnlein,[7] D. Bogert,[7] S. Cavanaugh,[9] D. Cherdack,[27] S. Childress,[7] B. C. Choudhary,[7] J. A. B. Coelho,[6] S. J. Coleman,[29] L. Corwin,[12] D. Cronin-Hennessy,[15] I. Z. Danko,[19] J. K. de Jong,[18] N. E. Devenish,[24] M. V. Diwan,[3] M. Dorman,[14] C. O. Escobar,[6] J. J. Evans,[14] E. Falk,[24] G. J. Feldman,[9] M. V. Frohne,[10] H. R. Gallagher,[27] R. A. Gomes,[8] M. C. Goodman,[1] P. Gouffon,[21] N. Graf,[11] R. Gran,[16] N. Grant,[20] K. Grzelak,[28] A. Habig,[16] D. Harris,[7] J. Hartnell,[24,20] R. Hatcher,[7] A. Himmel,[4] A. Holin,[14] X. Huang,[1] J. Hylen,[7] J. Ilic,[20] G. M. Irwin,[23] Z. Isvan,[19] D. E. Jaffe,[3] C. James,[7] D. Jensen,[7] T. Kafka,[27] S. M. S. Kasahara,[15] G. Koizumi,[7] S. Kopp,[26] M. Kordosky,[29] A. Kreymer,[7] K. Lang,[26] G. Lefeuvre,[24] J. Ling,[3,22] P. J. Litchfield,[15,20] R. P. Litchfield,[18] L. Loiacono,[26] P. Lucas,[7] W. A. Mann,[27] M. L. Marshak,[15] N. Mayer,[12] A. M. McGowan,[1] R. Mehdiyev,[26] J. R. Meier,[15] M. D. Messier,[12] D. G. Michael,[4,*] W. H. Miller,[15] S. R. Mishra,[22] J. Mitchell,[5] C. D. Moore,[7] J. Morfín,[7] L. Mualem,[4] S. Mufson,[12] J. Musser,[12] D. Naples,[19] J. K. Nelson,[29] H. B. Newman,[4] R. J. Nichol,[14] J. A. Nowak,[15] W. P. Oliver,[27] M. Orchanian,[4] R. Ospanov,[26] J. Paley,[1,12] R. B. Patterson,[4] G. Pawloski,[23] G. F. Pearce,[20] D. A. Petyt,[15] S. Phan-Budd,[1] R. K. Plunkett,[7] X. Qiu,[23] J. Ratchford,[26] T. M. Raufer,[20] B. Rebel,[7] P. A. Rodrigues,[18] C. Rosenfeld,[22] H. A. Rubin,[11] M. C. Sanchez,[13,1,9] J. Schneps,[27] P. Schreiner,[1] P. Shanahan,[7] C. Smith,[14] A. Sousa,[9] P. Stamoulis,[2] M. Strait,[15] N. Tagg,[17] R. L. Talaga,[1] J. Thomas,[14] M. A. Thomson,[5] G. Tinti,[18] R. Toner,[5] G. Tzanakos,[2] J. Urheim,[12] P. Vahle,[29] B. Viren,[3] A. Weber,[18] R. C. Webb,[25] C. White,[11] L. Whitehead,[3] S. G. Wojcicki,[23] T. Yang,[23] and R. Zwaska[7]

(MINOS Collaboration)

[1]*Argonne National Laboratory, Argonne, Illinois 60439, USA*
[2]*Department of Physics, University of Athens, GR-15771 Athens, Greece*
[3]*Brookhaven National Laboratory, Upton, New York 11973, USA*
[4]*Lauritsen Laboratory, California Institute of Technology, Pasadena, California 91125, USA*
[5]*Cavendish Laboratory, University of Cambridge, Madingley Road, Cambridge CB3 0HE, United Kingdom*
[6]*Universidade Estadual de Campinas, IFGW-UNICAMP, CP 6165, 13083-970, Campinas, SP, Brazil*
[7]*Fermi National Accelerator Laboratory, Batavia, Illinois 60510, USA*
[8]*Instituto de Física, Universidade Federal de Goiás, CP 131, 74001-970, Goiânia, GO, Brazil*
[9]*Department of Physics, Harvard University, Cambridge, Massachusetts 02138, USA*
[10]*Holy Cross College, Notre Dame, Indiana 46556, USA*
[11]*Physics Division, Illinois Institute of Technology, Chicago, Illinois 60616, USA*
[12]*Indiana University, Bloomington, Indiana 47405, USA*
[13]*Department of Physics and Astronomy, Iowa State University, Ames, Iowa 50011 USA*
[14]*Department of Physics and Astronomy, University College London, Gower Street, London WC1E 6BT, United Kingdom*
[15]*University of Minnesota, Minneapolis, Minnesota 55455, USA*
[16]*Department of Physics, University of Minnesota–Duluth, Duluth, Minnesota 55812, USA*
[17]*Otterbein College, Westerville, Ohio 43081, USA*
[18]*Subdepartment of Particle Physics, University of Oxford, Oxford OX1 3RH, United Kingdom*
[19]*Department of Physics and Astronomy, University of Pittsburgh, Pittsburgh, Pennsylvania 15260, USA*
[20]*Rutherford Appleton Laboratory, Science and Technologies Facilities Council, OX11 0QX, United Kingdom*
[21]*Instituto de Física, Universidade de São Paulo, CP 66318, 05315-970, São Paulo, SP, Brazil*
[22]*Department of Physics and Astronomy, University of South Carolina, Columbia, South Carolina 29208, USA*
[23]*Department of Physics, Stanford University, Stanford, California 94305, USA*
[24]*Department of Physics and Astronomy, University of Sussex, Falmer, Brighton BN1 9QH, United Kingdom*
[25]*Physics Department, Texas A&M University, College Station, Texas 77843, USA*
[26]*Department of Physics, University of Texas at Austin, 1 University Station C1600, Austin, Texas 78712, USA*
[27]*Physics Department, Tufts University, Medford, Massachusetts 02155, USA*
[28]*Department of Physics, Warsaw University, Hoża 69, PL-00-681 Warsaw, Poland*
[29]*Department of Physics, College of William & Mary, Williamsburg, Virginia 23187, USA*

(Received 2 March 2011; published 2 May 2011)

Measurements of neutrino oscillations using the disappearance of muon neutrinos from the Fermilab NuMI neutrino beam as observed by the two MINOS detectors are reported. New analysis methods have been applied to an enlarged data sample from an exposure of 7.25×10^{20} protons on target. A fit to neutrino oscillations yields values of $|\Delta m^2| = (2.32^{+0.12}_{-0.08}) \times 10^{-3}$ eV^2 for the atmospheric mass splitting

and $\sin^2(2\theta) > 0.90$ (90% C.L.) for the mixing angle. Pure neutrino decay and quantum decoherence hypotheses are excluded at 7 and 9 standard deviations, respectively.

DOI: 10.1103/PhysRevLett.106.181801 PACS numbers: 14.60.Pq, 14.60.Lm, 29.27.−a, 29.40.Mc

Neutrino masses and flavor mixing influence the role of neutrinos in fundamental physics processes [1] and may point to the mechanism that gives rise to the matter-antimatter asymmetry in the Universe [2]. A variety of phenomena observed with neutrinos originating in Earth's atmosphere or the Sun and those produced by nuclear reactors or accelerators exhibit quantum-mechanical mixing of the weak flavor eigenstates of neutrinos. The resulting neutrino oscillations, well established by several experiments over the past decade [3–7], are governed by the 3×3 unitary Pontecorvo-Maki-Nakagawa-Sakata (PMNS) matrix [8], which can be parametrized using three mixing angles and a CP-violating phase. Evolution of neutrino flavor eigenstates in vacuum depends additionally on the ratio of the distance traveled to the neutrino energy (L/E) and the splitting between the squared masses of neutrino mass eigenstates i and j, $\Delta m^2_{ji} = m^2_j - m^2_i$. For three neutrinos there are two independent mass splittings. MINOS, a long-base-line experiment with $L/E = \mathcal{O}(500\ \mathrm{km/GeV})$, is sensitive to the larger (atmospheric) mass splitting through the disappearance of muon neutrinos [9].

MINOS uses two detectors separated by a distance of 734 km, and the intense NuMI neutrino beam from Fermilab [10]. The Near Detector (ND) primarily characterizes the beam near its production. The Far Detector (FD) measures the event rate and energy spectra after the neutrinos have traveled through Earth's crust. MINOS presented earlier [4] the most precise measurement to date of the atmospheric mass splitting from a beam exposure of 3.36×10^{20} protons on target (POT). The results in this Letter are based on an exposure of 7.25×10^{20} POT, involve additional event categories, and employ an improved analysis methodology.

The beam [10] uses 120 GeV/c protons directed onto a graphite target of two interaction lengths. Positively charged secondary hadrons are focused towards the beam axis by two magnetic horns. The neutrino beam is the product of pion, kaon, and muon decays downstream of the target, primarily along a 675 m long decay pipe, evacuated for the first half of the data set [4], but later filled with 0.9 atm helium for structural reasons. Data taken at different relative horn-target longitudinal positions and horn currents were used to tune the neutrino beam simulation [11]. The effect of the helium in the decay pipe and an observed decrease in neutrino flux per POT, attributed to target degradation, are incorporated into the modeling. Most of the data were collected with the target placed in the most downstream position, yielding an event energy spectrum peaking at 3 GeV. A small amount of the data was taken with the target placed upstream, in the high energy configuration, which yields an energy spectrum that peaks at 9 GeV.

Both MINOS detectors [12,13] are placed along the beam axis. Each is a tracking, sampling calorimeter, built of 2.54 cm thick iron plates interleaved with scintillator planes composed of 1 cm thick, 4.1 cm wide scintillator strips, arranged in two alternating orthogonal views and read out using multianode photomultipliers. The ND is located 1.04 km downstream from the target and has a 23.7 ton fiducial mass. The FD has a 4.2 kton fiducial (5.4 kton total) mass. Both detectors have a toroidal magnetic field oriented to focus negatively charged particles.

In comparison to the previous analysis [4], the data set has been substantially increased and the simulation, reconstruction, and analysis methodology have been improved. This analysis also benefits from relaxed muon track charge selection and from incorporating events originating outside of the fiducial volume, including the surrounding rock. The geometrical modeling of the target and the beam focusing system have been improved [14]. The simulation uses the FLUGG software package [15] which combines GEANT4 [16] geometry with the FLUKA [17] hadron production. As previously, the detector simulation uses GEANT3 with NEUGEN3 [18] as the neutrino interaction generator.

The most significant analysis improvement is achieved by the new energy estimator of showers produced by low energy hadronic cascades. The new method relies on a k-nearest-neighbor (k-NN) algorithm [19]. In MINOS, a charged current (CC) interaction of a muon neutrino is characterized by a muon track and a hadronic cascade, reconstructed as one or more showers. The energy resolution of events is usually limited by the calorimetric measurement of the showers, which has a resolution of $56\%/\sqrt{E(\mathrm{GeV})} \oplus 2\%$ [12]. This can be compared to a resolution of 4.6% (11%) for 3 GeV muon tracks measured by range (curvature). The new hadronic energy estimator uses three event characteristics: the summed reconstructed energy deposited by showers within 1 m of the track vertex, the sum of the energy in the largest two reconstructed showers associated with the event, and the length of the longest shower [20]. The hadronic energy is taken as the mean true hadronic energy of the closest Monte Carlo events in this three-dimensional feature space. Monte Carlo studies show that the new algorithm improves shower energy resolution, e.g., from 55% to 43% for showers between 1.0–1.5 GeV.

The muon neutrino CC selection uses the energy deposition and its fluctuation along a track to discriminate muon tracks from spurious tracks reconstructed from hadronic

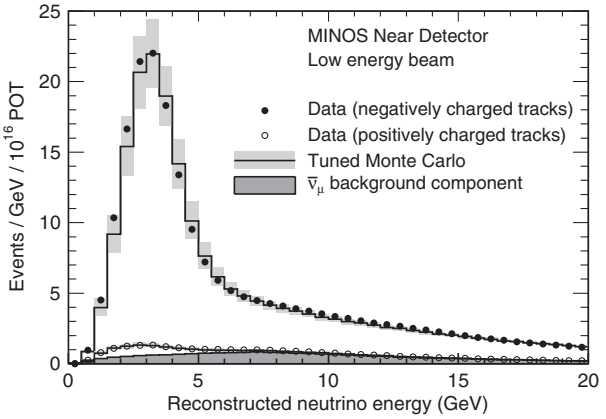

FIG. 1. The energy spectra of fully reconstructed events in the ND classified as CC interactions. The solid and open circles show the data reconstructed with negative or positive track charge, respectively. The solid lines show the tuned Monte Carlo calculations with a shaded error band due to systematic uncertainties. The shaded area at the bottom represents the simulated antineutrino component.

activity in neutral current (NC) interactions [4,21]. However, this method does not resolve events with muons crossing 10 or fewer detector planes (corresponding to about 500 MeV muon energy). An additional procedure reclaims some of these events by constructing a new muon classifier, also based on the k-NN method. It uses the total pulse height of the last 5 scintillator strips associated with a track, and two quantities that are correlated with track scattering [22]. The new selection achieves a 90% CC efficiency. Below 2 GeV, the efficiency is 77% with 6.5% NC contamination.

Events classified as CC interactions are used irrespective of the reconstructed charge sign of the track. Compared to the previous analysis [4], which used only events with a well-identified negative track charge, events at low energy, where track charge-sign reconstruction is less reliable, have now been recovered. Below 6 GeV, the main oscillation energy range, 98.0% of all selected events arise from neutrino interactions; the antineutrino component, shown in Fig. 1, is small and contributes primarily at higher energies. These antineutrinos are assumed to oscillate with the same parameters as the neutrinos.

The predicted energy spectrum in the FD is calculated from the spectrum measured in the ND [11]. The ND events with tracks of positive and negative reconstructed charges are used separately to provide energy spectra predictions at the FD [23,24]. The FD events with a reconstructed negative track charge are further divided into five quantiles based on energy resolution [24] determined by simulations and test beam measurements [13]. This division increases the sensitivity with which MINOS can measure neutrino oscillations [25], since events with the most precisely reconstructed energy are the most effective in determining the CC disappearance.

This analysis includes interactions originating in the rock and outside the FD fiducial volume. Such interactions are only partially reconstructed, and are characterized by the measured muon and its detector entry position [26,27]. The predicted energy spectrum for these events is derived using the same method as for the fully reconstructed events. The partially and fully reconstructed samples have comparable statistics, but the partially reconstructed events contribute primarily to establishing the overall event rate since they are not well measured and are predominantly at higher energies.

The effect of systematic uncertainties on the measured oscillation parameters was determined using Monte Carlo simulations in which modeling parameters were varied. Table I shows the systematic effects, their 1 standard deviation level, and the impact on the values of mass splitting and mixing angle. Uncertainties in the physics simulations, including pion absorption cross sections in the nucleus and associated modeling of energy deposition in the detector, result in the uncertainty in the visible hadronic energy (a), which is energy dependent and is about 7.0% below 3 GeV.

TABLE I. Sources of systematic uncertainties and their impact on fitting oscillation parameters.

Source of systematic uncertainty	$\delta(\Delta m^2)$ (10^{-3} eV^2)	$\delta[\sin^2(2\theta)]$
(a) Hadronic energy	0.051	<0.001
(b) μ energy (range 2%, curv. 3%)	0.047	0.001
(c) Relative normalization (1.6%)	0.042	<0.001
(d) NC contamination (20%)	0.005	0.009
(e) Relative hadronic energy (2.2%)	0.006	0.004
(f) $\sigma_\nu(E_\nu < 10$ GeV)	0.020	0.007
(g) Beam flux	0.011	0.001
(h) Neutrino-antineutrino separation	0.002	0.002
(i) Partially reconstructed events	0.004	0.003
Total systematic uncertainty	0.085	0.013
Expected statistical uncertainty	0.124	0.060

TABLE II. Numbers of events classified in the FD as fully and partially reconstructed CC interactions shown for all running periods. The predicted numbers are calculated under the assumption of no oscillations.

Run period	POT (10^{20})	Predicted (no oscillations)		Observed (FD)	
		Fully	Partially	Fully	Partially
I	1.269	426	375	318	357
II	1.943	639	565	511	555
III	3.881	1252	1130	1037	977
High energy	0.153	134	136	120	128
Total	7.246	2451	2206	1986	2017

The errors in the measurement of muon energy (b) from range (2% error) or from curvature in the magnetic field (3%) are included. The effects of relative reconstruction efficiencies between the two detectors and uncertainties in their fiducial masses and relative difference in detector structure result in the 1.6% normalization error (c). The largest uncertainty in the mixing angle is from the amount of NC background (d), the uncertainty on which, based on a data-driven method, is 20% [22]. Other sources of uncertainty include the 2.2% relative energy calibration uncertainty between the two detectors (e), uncertainties in the neutrino cross sections σ_ν (f), the beam flux (g), and uncertainties due to misclassification of neutrino and antineutrino interactions (h). Finally, incorporation of partially reconstructed events introduces a small uncertainty due to approximations made in modeling the rock composition and details of the FD edges (i).

All event selection criteria and analysis procedures were defined prior to examining the full data set in the FD. The energy spectra obtained by the new analysis agreed well with those from the previous publication [4], within small differences expected due to changes in the reconstruction algorithm. Table II shows event statistics. The energy spectrum of the fully reconstructed FD data sample is shown in Fig. 2, along with the predicted spectra. The corresponding spectra for the partially reconstructed events are shown in Fig. 3.

The two-parameter survival probability formula $P(\nu_\mu \to \nu_\mu) = 1 - \sin^2(2\theta)\sin^2(\Delta m^2 L/4E)$ was used to test the neutrino oscillation model. The best values of $|\Delta m^2|$ and $\sin^2(2\theta)$ were found by maximizing a likelihood, which includes the four dominant systematic uncertainties (a)–(d) in Table I as nuisance fit parameters [28,29]. The likelihood value is computed at each point in the $|\Delta m^2| - \sin^2(2\theta)$ plane by summing the contributions from the seven event categories: five (one) bins of energy resolution for fully reconstructed events with

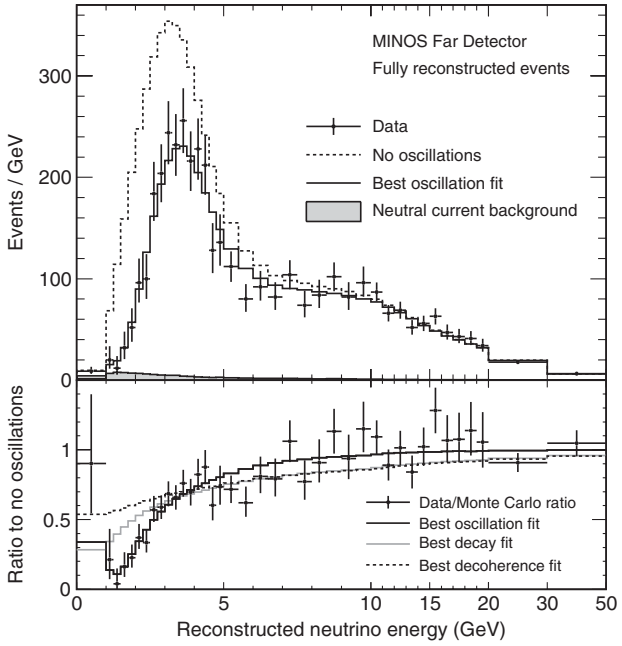

FIG. 2. Top: The energy spectra of fully reconstructed events in the FD classified as CC interactions. The dashed histogram represents the spectrum predicted from the ND assuming no oscillations, while the solid histogram reflects the best fit of the oscillation hypothesis. The shaded area shows the predicted NC background. Bottom: The points with error bars are the background-subtracted ratios of data to the no-oscillation hypothesis. Lines show the best fits for oscillations, decay [30], and decoherence [31].

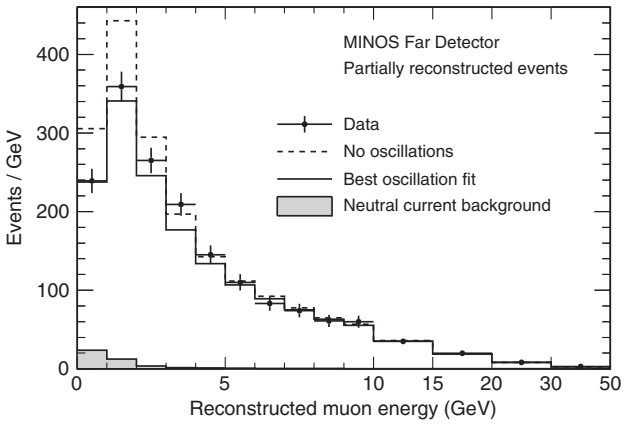

FIG. 3. The muon energy spectra of partially reconstructed events in the FD. Conventions as in Fig. 2.

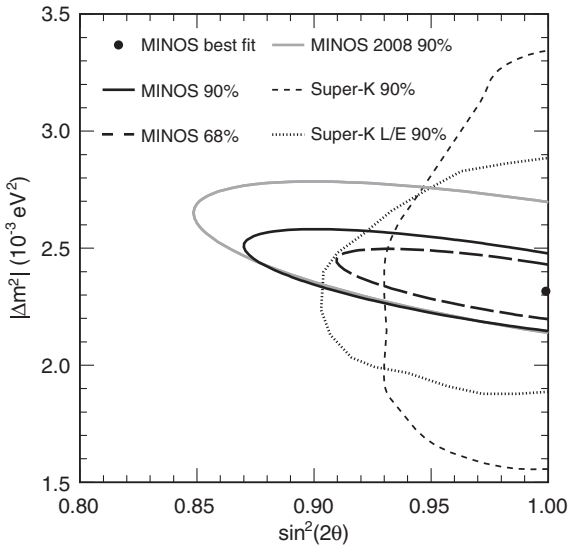

FIG. 4. Likelihood contours of 68% and 90% C.L. around the best fit values for the mass splitting and mixing angle. Also shown are contours from previous measurements [3,4].

negative (positive) tracks, and partially reconstructed events. Within each category the likelihood value is calculated by comparing the observed energy spectrum with that predicted for the oscillation parameters of that point. The best fit value and one-dimensional uncertainties for the mass splitting are $|\Delta m^2| = (2.32^{+0.12}_{-0.08}) \times 10^{-3}$ eV^2. For the mixing angle, if $\sin^2(2\theta)$ is constrained to be ≤ 1, the best fit is $\sin^2(2\theta) = 1.00$ or $\sin^2(2\theta) > 0.94$ (0.90) at 68% (90)% C.L. The best fit values with the resulting 68% and 90% C.L. contours are shown in Fig. 4; 41% of mock experiments with the same statistics would have a smaller likelihood. The physical boundary on $\sin^2(2\theta)$ results in the smaller uncertainty than expected from the simulated sensitivity. Without this constraint the best fit value for mass splitting changes by $\delta(\Delta m^2) = -0.01 \times 10^{-3}$ eV^2 and the mixing angle changes by $\delta[\sin^2(2\theta)] = +0.001$. The fits do not significantly pull away from their nominal values any of the four nuisance parameters. The predicted energy spectrum for the best fit is shown in Fig. 2. If the fit is restricted to use only fully reconstructed events with the negative track charge, the best fit value for mass splitting changes by $\delta(\Delta m^2) = +0.03 \times 10^{-3}$ eV^2 and the mixing angle is unchanged. Two other hypotheses for neutrino disappearance, pure decay [30] and pure quantum decoherence [31], are excluded at 7 and 9 standard deviations, respectively, as shown in Fig. 2.

In summary, MINOS data from a beam exposure of 7.25×10^{20} POT with an improved analysis have resulted in the measurement of the atmospheric mass splitting of $|\Delta m^2| = (2.32^{+0.12}_{-0.08}) \times 10^{-3}$ eV^2 and mixing angle of $\sin^2(2\theta) > 0.90$ (90% C.L.). This is the most precise measurement of this mass splitting to date. Neither the pure quantum decoherence nor neutrino decay hypotheses fit the observed spectra.

This work was supported by the U.S. DOE, the UK STFC, the U.S. NSF, the State and University of Minnesota, the University of Athens, Greece, and Brazil's FAPESP, CNPq, and CAPES. We are grateful to the Minnesota DNR, the crew of the Soudan Underground Laboratory, and the personnel of Fermilab for their contributions to this effort.

*Deceased.

[1] R. N. Mohapatra and A. Y. Smirnov, Annu. Rev. Nucl. Part. Sci. **56**, 569 (2006).
[2] M. Fukugita and T. Yanagida, Phys. Lett. B **174**, 45 (1986); S. Davidson, E. Nardi, and Y. Nir, Phys. Rep. **466**, 105 (2008).
[3] Y. Ashie *et al.*, Phys. Rev. Lett. **93**, 101801 (2004); Y. Ashie *et al.*, Phys. Rev. D **71**, 112005 (2005); J. Hosaka *et al.*, Phys. Rev. D **74**, 032002 (2006).
[4] P. Adamson *et al.*, Phys. Rev. Lett. **101**, 131802 (2008).
[5] B. Aharmim *et al.*, Phys. Rev. C **72**, 055502 (2005).
[6] S. Abe *et al.*, Phys. Rev. Lett. **100**, 221803 (2008).
[7] M. H. Ahn *et al.*, Phys. Rev. D **74**, 072003 (2006).
[8] B. Pontecorvo, JETP **34**, 172 (1958); V. N. Gribov and B. Pontecorvo, Phys. Lett. **28B**, 493 (1969); Z. Maki, M. Nakagawa, and S. Sakata, Prog. Theor. Phys. **28**, 870 (1962).
[9] The MINOS experiment measures an unresolved mixture of $|\Delta m^2_{31}|$ and $|\Delta m^2_{32}|$ which we refer to as $|\Delta m^2|$ for brevity. The parameter $\sin^2(2\theta)$ is likewise an admixture. For further discussion, see G. Fogli *et al.*, Prog. Part. Nucl. Phys. **57**, 742 (2006).
[10] S. Kopp, in *Proceedings of the 2005 IEEE Particle Accelerator Conference, Knoxville, TN* (IEEE, Piscataway, NJ, 2005).
[11] P. Adamson *et al.*, Phys. Rev. D **77**, 072002 (2008).
[12] D. Michael *et al.*, Nucl. Instrum. Methods Phys. Res., Sect. A **596**, 190 (2008).
[13] P. Adamson *et al.*, Nucl. Instrum. Methods Phys. Res., Sect. A **556**, 119 (2006); A. Cabrera *et al.*, Nucl. Instrum. Methods Phys. Res., Sect. A **609**, 106 (2009).
[14] Ž. Pavlović, Ph.D. thesis, University of Texas at Austin, 2008.
[15] G. Battistoni *et al.*, AIP Conf. Proc. **896**, 31 (2007).
[16] S. Agostinelli *et al.*, Nucl. Instrum. Methods Phys. Res., Sect. A **506**, 250 (2003).
[17] F. Ballarini *et al.*, J. Phys. Conf. Ser. **41**, 151 (2006).
[18] S. Dytman, H. Gallagher, and M. Kordosky, arXiv:0806.2119.
[19] T. M. Cover and P. E. Hart, IEEE Trans. Inf. Theory **13**, 21 (1967).
[20] C. Backhouse, D.Phil. thesis, University of Oxford, 2011.
[21] R. Ospanov, Ph.D. thesis, University of Texas at Austin, 2008.
[22] J. Ratchford, Ph.D. thesis, University of Texas at Austin, 2011.
[23] J. Evans, D.Phil. thesis, University of Oxford, 2008.
[24] S. Coleman, Ph.D. thesis, College of William & Mary, 2011.
[25] J. Marshall, Ph.D. thesis, University of Cambridge, 2008.

[26] A. McGowan, Ph.D. thesis, University of Minnesota, 2007.
[27] M. Strait, Ph.D. thesis, University of Minnesota, 2010.
[28] W. A. Rolke, A. M.Lopez, and J. Conrad, Nucl. Instrum. Methods Phys. Res., Sect. A **551**, 493 (2005).
[29] J. Mitchell, Ph.D. thesis, University of Cambridge, 2011.
[30] V. D. Barger *et al.*, Phys. Lett. B **462**, 109 (1999).
[31] E. Lisi, A. Marrone, and D. Montanino, Phys. Rev. Lett. **85**, 1166 (2000).